Mechanism for Hydrothermal Synthesis of LiFePO4 Platelets as Cathode Material for Lithium-Ion Batteries

ARTICLE *in* THE JOURNAL OF PHYSICAL CHEMISTRY C · SEPTEMBER 2010

Impact Factor: 4.77 · DOI: 10.1021/jp104466e

6 AUTHORS, INCLUDING:

Xiaohui Wang
Chinese Academy of Sciences
71 PUBLICATIONS **2,058** CITATIONS
SEE PROFILE

Huimin Xiang
Aerospace Research institute of material a…
28 PUBLICATIONS **156** CITATIONS
SEE PROFILE

Yanchun Zhou
Aerospace Research Institute of Materials …
400 PUBLICATIONS **7,872** CITATIONS
SEE PROFILE

Mechanism for Hydrothermal Synthesis of $LiFePO_4$ Platelets as Cathode Material for Lithium-Ion Batteries

Xue Qin,[†,‡] Xiaohui Wang,[*,†] Huimin Xiang,[†,‡] Jie Xie,[†,‡] Jingjing Li,[†,‡] and Yanchun Zhou[†]

High-Performance Ceramic Division, Shenyang National Laboratory for Materials Science, Institute of Metal Research, Chinese Academy of Sciences, 72 Wenhua Road, Shenyang 110016, China, and Graduate School of Chinese Academy of Sciences, Beijing 100039, China

Received: May 17, 2010; Revised Manuscript Received: August 15, 2010

The low-temperature hydrothermal synthesis method has been drawing ever-growing attention due to the fact that it has many advantages over conventional methods for preparing promising cathode material $LiFePO_4$. However, the mechanism for hydrothermal synthesis of $LiFePO_4$ remains unclear. Here, the hydrothermal reaction mechanism of $LiFePO_4$ is systematically studied by X-ray diffraction (XRD), scanning electron microscopy (SEM), transmission electron microscopy (TEM), Fourier transform infrared spectroscopy (FTIR), and specific surface analysis. As evidenced by apparent precursor dissolution, fast hydrothermal formation, and significant decrease in particle size with adding alcohols and/or carbon black in the reaction system, a dissolution−precipitation mechanism accounts for the hydrothermal synthesis of $LiFePO_4$. Moreover, we identified tetraphosphate in the $LiFePO_4$ precursor. This compound undergoes hydrolysis upon heating during the hydrothermal process, resulting in a remarkable decline of pH value.

1. Introduction

In the field of lithium-ion battery research, tremendous efforts have been put into finding alternatives to the toxic and expensive cobalt-oxide-based cathodes currently employed in commercialized lithium-ion batteries, particularly for potential use in large-scale applications such as hybrid electric vehicles (HEV).[1−4] $LiFePO_4$, whose electrochemical activities were first reported by Pahdi et al.,[1] has become a highly promising cathode material for use in lithium-ion batteries because of its advantages such as high voltage (3.4 V vs Li/Li^+) and large theoretical capacity (170 $mAh \cdot g^{-1}$), as well as its low cost, high safety, and nontoxicity. Unlike $LiCoO_2$, which forms a solid solution during charge and discharge, and therefore demonstrates sloping charge and discharge curves,[5−7] $LiFePO_4$ undergoes a two-phase transition between $LiFePO_4$ and $FePO_4$ during charge/discharge with a rather flat voltage profile. The mechanism of $LiFePO_4$ transition into isostructural $FePO_4$ has been elucidated using transition electron microscopy (TEM). It was demonstrated that lithium was extracted at narrow, disordered transition zones on the *ac* crystal surface as the phase boundary progresses in the direction of the *a* axis.[8]

Very recently, Allen et al.[9] investigated the electrochemical phase transformation of carbon-coated $LiFePO_4$ nanophase by use of the Avrami−Johnson−Mehl−Eroofev equation. They obtained an Avrami exponent equal to 1, which is indicative of one-dimensional growth. This result does not support the conventional shrinking core model for the electrochemical conversion of $FePO_4$ to $LiFePO_4$. Moreover, analysis of the exponent reveals that the phase transition is controlled by a phase boundary reaction rather than by diffusion. Chen et al.[8] suggested that reducing the crystal size along the *b* axis would improve the electrochemical properties of the materials toward Li^+ extraction/insertion. This has been proved in the platelike $LiFePO_4$ crystals prepared hydrothermally, which exhibited a higher electrochemical reactivity.[10]

$LiFePO_4$ cathode materials have been produced by a variety of methods, such as a sol−gel process,[11] carbothermal reduction method,[12,13] and hydrothermal synthesis.[14,15] Among these methods, hydrothermal synthesis has some advantages such as simplicity, homogeneous particle size distribution, greater electrochemical performances and cycle life, morphology control, and low cost.[14−24] However, to the best of our knowledge, the formation mechanism of the phospholivines under hydrothermal conditions is not fully understood.

This work reports the formation mechanism of $LiFePO_4$ platelets under hydrothermal synthesis conditions. A dissolution−precipitation mechanism accounts for the hydrothermal synthesis of $LiFePO_4$, as evidenced by three experimental observations: apparent precursor dissolution, fast hydrothermal formation of $LiFePO_4$, and significant decease in particle size upon the addition of alcohols and carbon black in the reaction system. According to this mechanism, a strategy is pointed out to further improve the electrochemical properties of hydrothermally prepared $LiFePO_4$ platelates as cathode material for lithium-ion batteries.

2. Experimental Section

2.1. Synthesis of $LiFePO_4$. All the chemicals (AR grade) were purchased from Sinopharm Chemical Reagent. The precursor of $LiFePO_4$ was prepared as follows: 4.1703 g of $FeSO_4 \cdot 7H_2O$, 1.7239 g of H_3PO_4 (85 wt. %), and 0.2 g of ascorbic acid were dissolved in 50 mL of deionized water under magnetic stirring to obtain a solution. A 1.8882 g portion of $LiOH \cdot H_2O$ was dissolved in another beaker with 30 mL of deionized water under magnetic stirring, which was then slowly added to the above solution to keep the molar ratio Li:Fe:P = 3:1:1. With the addition of LiOH solution, a mass of sticky mixture was formed. The resulting mixture, i.e., precursor, was

* Corresponding author. Fax: +86 24 23891320. Phone: +86 24 83970549. E-mail: wang@imr.ac.cn.

† High-Performance Ceramic Division, Shenyang National Laboratory for Materials Science, Institute of Metal Research, Chinese Academy of Sciences.

‡ Graduate School of Chinese Academy of Sciences.

10.1021/jp104466e
Published on Web 09/02/2010

quickly transferred into a 90-mL-capacity stainless steel autoclave without Teflon lining and sealed to prevent the precursor from being oxidized. The sealed autoclave was then placed into a silicon oil bath, and heated up to 100−180 °C for 0−180 min under magnetic stirring. Subsequently, the autoclave was cooled down to room temperature in the oil bath. The supernatant in the autoclave was collected for pH measurement. Precipitate was collected by suction filtration and was washed several times with deionized water.

2.2. Characterization. The precipitates were characterized by powder XRD (Rigaku D/max-2400), FTIR (PerkinElmer), SEM (LEO, Oberkochen), TEM (FEI, Tecnai G^2 20), and Brunauer−Emmett−Teller surface analysis (BET; Micromeritics Inc., ASAP 2020) with nitrogen as adsorption gas at 77 K. The particle size distribution of the samples was determined by using an acoustic and electroacoustic spectrometer (DT-1200, Dispersion Technology Inc., Bedford Hills). The pH values of the supernatants were measured by microprocessor pH meter (PHs-3cw, LIPA).

2.3. Electrochemical Tests. Electrochemical measurements were carried out using a 2032-type coin cell. The electrolyte was a 1 M solution of $LiPF_6$ in 1:1:1 (v/v/v) ethylene carbonate/dimethyl carbonate/ethylmethyl carbonate. The counter electrode was a disk of lithium metal foil (18 mm in diameter, 0.5 mm thick). A polypropylene membrane was used as a separator. For cathode preparation, the synthesized $LiFePO_4$ powders were first mixed with glucose at a ratio of 1:0.4 (w/w), followed by heating at 700°C for 2 h in an Ar atmosphere containing 7 vol % H_2 to obtain a cathode composite containing $LiFePO_4$ and carbon. The working electrode was 80:10:10 (w/w/w) cathode composite/acetylene black/ poly(vinylidene fluoride). Galvanostatic charging−discharging experiments were carried out on LAND CT2001A cycler (Wuhan Kingnuo Electronic Co.) in the voltage range 2.0−4.2 V.

3. Results

3.1. Measurement of in Situ Reaction Temperature. Previous reports on the hydrothermal synthesis of $LiFePO_4$ always regarded heater temperature as reaction temperature.[14−24] For hydrothermal synthesis using aqueous solution as reaction medium, there should be a significant temperature difference between the heater and the inner reaction system because of the high specific heat capacity of the aqueous solution. To get the accurate reaction temperature during the hydrothermal synthesis of $LiFePO_4$, a thermal couple was inserted into the autoclave, allowing us to simultaneously record the oil bath and autoclave inner temperatures. Figure 1 shows the time dependence of recorded temperatures of oil bath and autoclave inner for the precursor hydrothermally reacted at oil bath temperatures of 165 and 180 °C without holding time and 180 °C for 5 min under oil-bath-cooled condition [denoted as LFP-165, LFP-180, and LFP-180(5)], respectively. Evidently, the temperature difference between the oil bath and the autoclave inner is remarkable although our stainless steel autoclave without Teflon lining has higher thermal conductivity than a conventional Teflon-lined vessel. It is thereby suggested that the temperature difference between the heater and aqueous solution reaction system should be considered for a more accurate description of the mechanism.

3.2. Phase Evolution. To understand phase evolution of precursor with temperature, the precursor was treated by immersing the autoclave in the oil bath which was heated from room temperature up to temperatures ranging from 100 to 180 °C. The treated samples were collected and subjected to powder XRD examinations. Figure 2 shows the powder XRD patterns

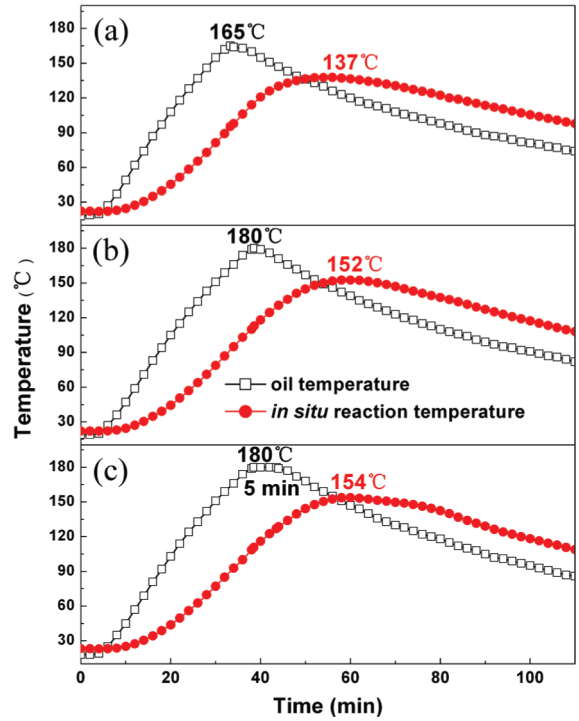

Figure 1. Comparisons of in situ reaction and oil temperatures against time for precursor reacted hydrothermally at oil temperature of (a) 165 °C without holding time, (b) 180 °C without holding time, and (c) 180 °C for 5 min.

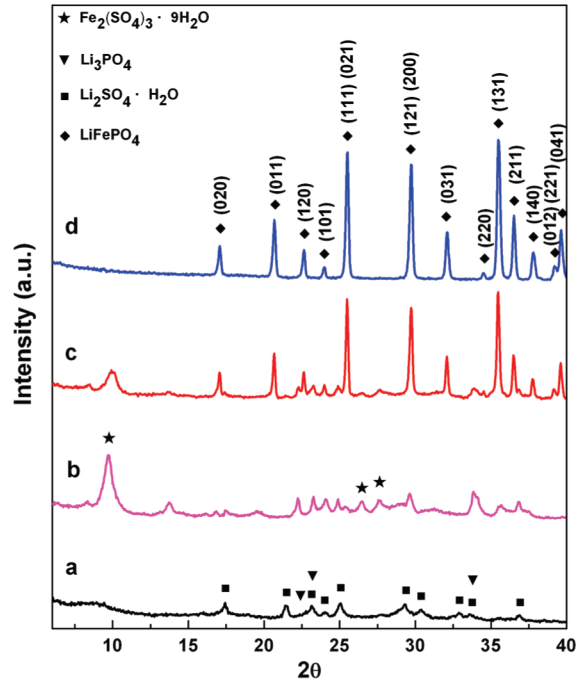

Figure 2. Powder XRD patterns of (a) precursor, (b) those reacted at oil temperature of 165 °C without holding time, (c) those reacted at 180 °C without holding time, and (d) those reacted at 180 °C for 5 min.

of the precursor, LFP-165, LFP-180, and LFP-180(5). The precursor consists of several crystalline phases corresponding to Li_3PO_4 and $Li_2SO_4 \cdot H_2O$. Relatively weak and disordered reflection of the precursor demonstrates the existence of amorphous phases. $Fe_2(SO_4)_3 \cdot 9H_2O$, an oxidation state of $FeSO_4$,[25] is identified in the XRD pattern of LFP-165, indicating the existence of unreacted $FeSO_4$. Surprisingly, phase-pure

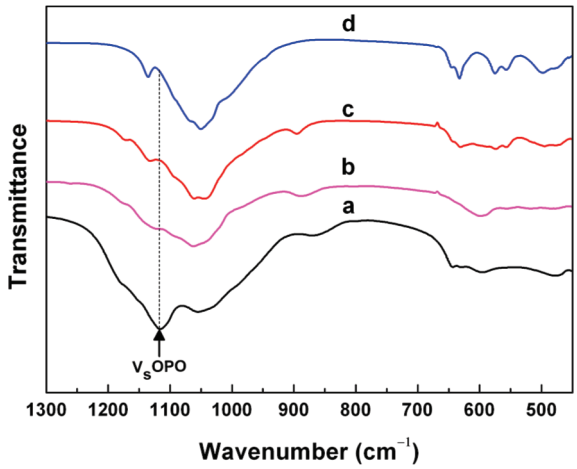

Figure 3. FTIR spectra of (a) precursor, (b) LFP-165, (c) LFP-180, and (d) LFP-180(5) in the range 450−1300 cm^{-1} at room temperature.

$LiFePO_4$ was formed as soon as the in situ reaction temperature increased to a temperature as low as 154 °C. Such quick formation of $LiFePO_4$, to the best knowledge of the present authors, is reported for the first time.

XRD is a powerful tool for characterizing crystalline phases. It is, however, not suitable for amorphous phases. Thus, we employed FTIR to further investigate the phase evolution with temperature. Figure 3 shows the FTIR spectra of the precursor, LFP-165, LFP-180, and LFP-180(5) in the wavenumber range 450−1300 cm^{-1}. One striking feature for the spectrum of the precursor is the presence of a strong absorption at 1116 cm^{-1}. This absorption is attributed to the symmetric stretching vibration mode of O−P−O (V_s-OPO) in tetraphosphate compounds.[26,27] Similarly, during the process of study on phase evolution of hydrothermally synthesized $LiMnPO_4$, an alike strong absorption, as shown in Figure S1 (Supporting Information), was also observed. Furthermore, crystalline phosphate of Mn, and tetraphosphate in the form of tetraphosphate of Mn and Li, were presented in the XRD patterns (Figure S2, Supporting Information). Thus, it is proposed that amorphous iron tetraphosphate was formed by the addition of LiOH solution to a $FeSO_4$ and H_3PO_4 mixture solution containing ascorbic acid. This macromolecular compound leads to the precursor being sticky. As the reaction proceeded, the absorption corresponding to V_s-OPO gets faint, demonstrating that the amount of of $P_4O_{12}^{4-}$ decreases. The bending vibration modes of SO_4^{2-}, symmetric vibration mode of SO_4^{2-}, and asymmetric vibration mode of SO_4^{2-} appear at three bands at 590, 948, and 1029 cm^{-1}, respectively.[28] The reason for their disappearance is attributed to the removal of sulfate by washing with deionized water. The bands at 498, 557, 575, 633, 1050, and 1136 cm^{-1} are due to some vibration modes of PO_4^{3-} in $LiFePO_4$.[29−31] The bands at 1050 cm^{-1} is assigned to metal−PO_4^{3-} link vibration,[29] suggesting the existence of amorphous $Fe_3(PO_4)_2$ in the precursor.

3.3. Evolution of pH Value with Hydrothermal Treatment Time. According to the FTIR spectra (Figure 3), tetraphosphate compounds are present in the precursor while the final product only contains PO_4^{3-} species. Classical inorganic chemistry argues that the evolution from tetraphosphate compounds to PO_4^{3-} gives rise to the formation of H^+. To check whether this is the case in the present study, the percursor was, respectively, heated up to various temperatures followed by cooling down to room temperature in the oil bath. We then collected the supernatant and measured the pH values. Figure 4 shows the evolution of pH values of the supernatant with the corresponding

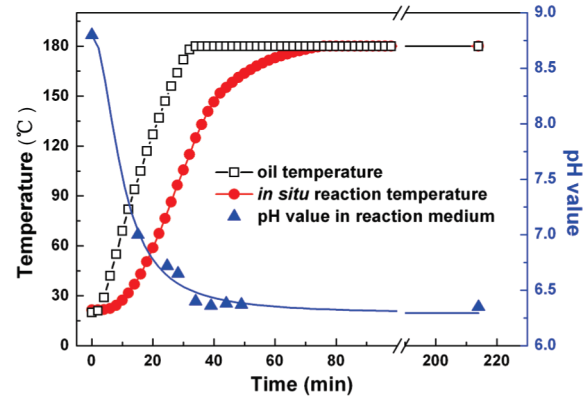

Figure 4. In situ monitoring of reaction temperature with variation of pH values of supernatant and the evolution of oil temperature during synthesis of $LiFePO_4$.

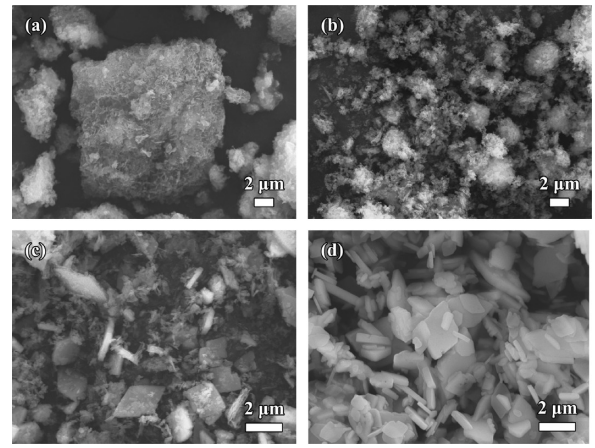

Figure 5. SEM images of (a) precursor, (b) LFP-165, (c) LFP-180, and (d) LFP-180(5).

oil bath and in situ reaction temperatures. It is apparent from Figure 4 that the pH values of the supernatants sharply drop with increase of in situ reaction temperature, which is consistent with the classical inorganic chemistry. Dokko et al.[10] have observed the pH value drop after hydrothermal treatment. However, a detailed explanation for the pH value drop is not available so far. Here, besides decomposition of ascorbic acid and increase of Li_2SO_4 as the reaction proceeded, we hold that the main reason for the drop originates from the hydrolysis of tetraphosphate consisting of a ring of four PO_4 tetrahedra linked by bridging oxygen under hydrothermal route.[32] Structure evolution of geometry of the anion tetraphosphate under hydrothermal conditions is shown in Scheme S1 (Supporting Information), and the hydrolysis equation is presented as the following equation:

$$P_4O_{12}^{4-} + 12H_2O \rightarrow 4PO_4^{3-} + 8H_3O^+ \quad (1)$$

A similar phenomenon was also observed during hydrothermal synthesis of $LiMnPO_4$, as shown in Figure S3 (Supporting Information).

3.4. Morphology Evolution. Figure 5 shows a series of typical morphologies from precursor to aim-product $LiFePO_4$. It can be clearly seen that there exists a precursor dissolving behavior from initial agglomerated structure (Figure 5a), to small aggregates consisting of an irregular sheetlike shape (Figure 5b), and finally to nanoleaflet structure for $LiFePO_4$ precursor (Figure 5c), until all precursor transforms to platelike $LiFePO_4$ powders

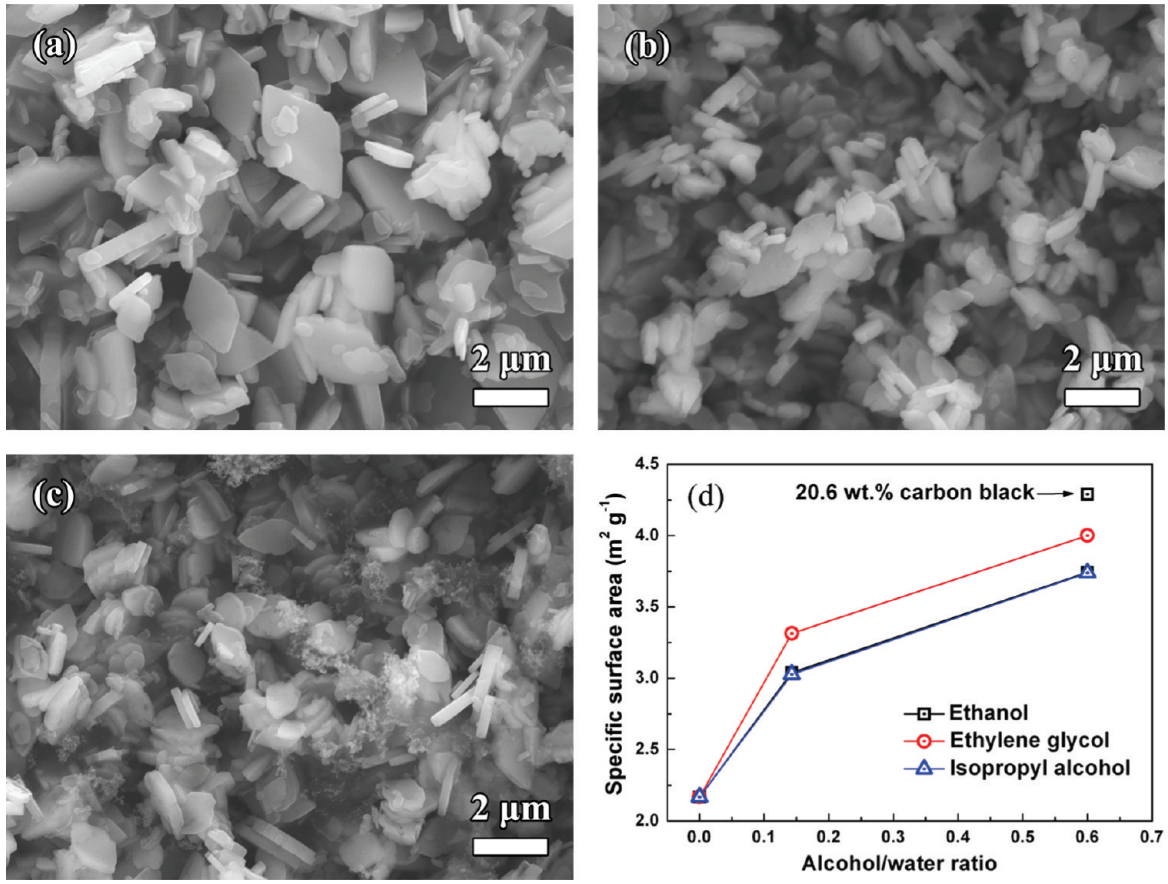

Figure 6. SEM images of $LiFePO_4$: (a) the precursor heated up to 180 °C for 3 h [LFP-180(3 h)], (b) with ethanol/water (3:5, v/v), (c) with ethanol/water (3:5, v/v) and carbon black (20.6 wt % vs $LiFePO_4$), and (d) the evolution of the specific surface areas for $LiFePO_4$ powders synthesized hydrothermally with various alcohols and contents in the reaction system and 20.6 wt % carbon black in reaction medium of ethanol/water (3:5, v/v).

(Figure 5d). These formations of nanoleaflet structure precursor are definitely understood through the mechanism of dissolution of the agglomerated precursor.[33] A similar precursor dissolution process for $LiMnPO_4$ was also observed in Figure S4 (Supporting Information). It is well acknowledged that three mechanisms are involved in the crystal formation and growth process under hydrothermal conditions. The three mechanisms include precipitation from supersaturated solution, in situ transformation, and dissolution−precipitation mechanism.[34−36] The mechanism of which is involved depends on the solubility of the precursor. In the present wok, since the solid precursor experienced a dissolution pocess, a dissolution−precipitation mechanism accounts for the hydrothermal synthesis of $LiFePO_4$.

3.5. Effects of Introducing Various Alcohols and/or Nucleation Sites. If the mechanism we proposed is correct, reducing the water content by adding alcohol and/or introducing nucleation sites with large specific surface area into the reaction medium should have a significant impact on the particle size of the obtained product.[37] To verify whether this is the case or not, various alcohols and/or carbon black were added into the reaction system to lower the solubility of the solutes and/or increase nucleation sites, respectively. The morphologies of the samples and corresponding specific surface areas are shown in Figure 6. Obviously, introducing ethanol into the hydrothermal reaction system reduces the particle size of $LiFePO_4$, as evidenced by the SEM images (Figure 6a,b). Similarly, compared with Figure 6b, introducing carbon black with a high specific surface area (62 $m^2 \cdot g^{-1}$) as nucleation sites further decreases the particle size of $LiFePO_4$ (Figure 6c). To further identify the effects of introducing various alcohols and/or adding carbon black, the synthesized samples were subjected to BET surface area measurements. Consistent with the morphologies observed by SEM, the measured specific surface areas for $LiFePO_4$ powders are increased with the addition of alcohol and carbon black, as can be seen from Figure 6d. Therefore, it is reasonable to draw a conclusion that dissolution−precipitation is the hydrothermal synthesis mechanism of $LiFePO_4$.

It is generally acknowledged that adding alcohol and/or introducing nucleation sites into a hydrothermal reaction medium could decrease particle size of hydrothermally prepared product, which is a characteristic for a dissolution−precipitation mechanism.[37] Adding alcohol into the hydrothermal reaction medium lowers the solubility of the $LiFePO_4$ precursor. As a result, supersaturation degree under hydrothermal conditions becomes higher, and nucleation rate is therefore increased.[38] In addition, introducing nucleation sites eases nucleation, leading to a greater number of nuclei formed. Thus, the particle size of hydrothermally prepared $LiFePO_4$ is reduced by adding alcohol and/or introducing nucleation sites into the hydrothermal reaction medium.

In contrast to the dissolution−precipitation mechanism, an in situ transformation mechanism needs much longer time because the diffusion of ions through the undissolved solid compound in the precursor and the reaction between the ions and undissolved compound are very slow.[39,40] In the present work, pure $LiFePO_4$ was formed as soon as the in situ reaction temperature increased to 154 °C, demonstrating that the hydrothermal synthesis process of $LiFePO_4$ is vey fast. It thereby could be perceived to be a process of rapid dissolution of precursor to yield insoluble species.

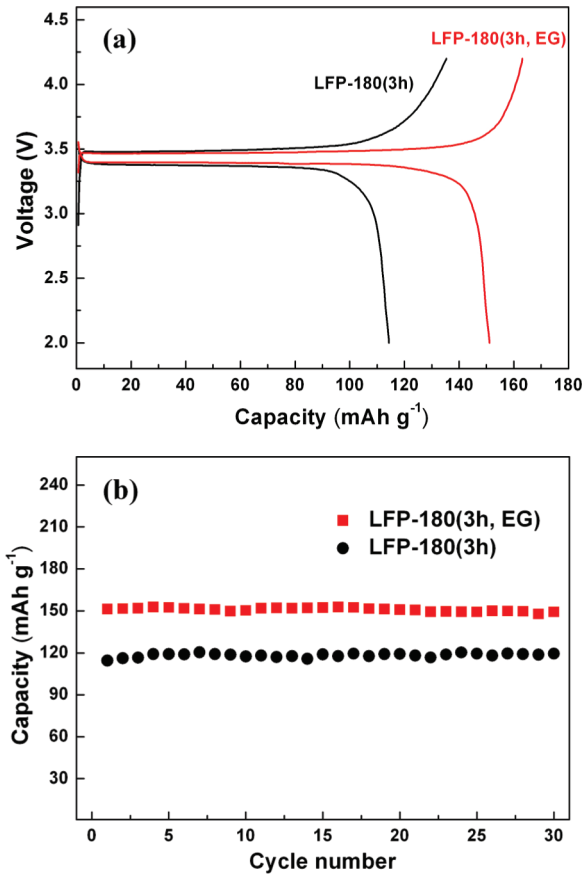

Figure 7. (a) Initial charge−discharge curves of LFP-180(3 h) and $LiFePO_4$ platelets prepared in ethylene glycol/water medium [3:5, v/v; LFP-180 (3 h, EG)] at 0.1 C charging and discharging rate and (b) their cycle performance.

In combination with the evidence in the form of phase analysis, pH value drop, morphology evolution, and effects of introducing various alcohols and/or nucleation sites, a dissolution−precipitation mechanism accounts for the hydrothermally prepared $LiFePO_4$ platelets.

3.6. Electrochemical Performance. It has been pointed out that adding various alcohols into the hydrothermal reaction system is an efficient way to reduce particle size. To check whether the particle size influences the electrochemical performance, we made electrochemical tests of the hydrothermally synthesized $LiFePO_4$ powders in different reaction media by using galvanostatic cycling. Figure 7a,b shows the initial charge−discharge curves and cycle performance of the LFP-180 (3 h) and LFP-180 (3 h, EG) at 0.1 C (17 mA/g) charge and discharge rate. It can be seen that the initial specific discharge capacity for LFP-180 (3 h) is 114 $mAh \cdot g^{-1}$, while that for LFP-180 (3 h, EG) approaches 151 $mAh \cdot g^{-1}$. Moreover, both have no significant capacity loss after 30 cycles, indicating that the cycling property for the hydrothermally synthesized $LiFePO_4$ is respectable.

The major reason for the improvement in the specific discharge capacity of LFP-180 (3 h, EG) is likely the reduced particle size. Previous studies have demonstrated that EG has a strong chelating ability for some transition metal ions.[41] Transition metal cations (e.g., Fe^{2+} in this study) could be trapped during the hydrothermal process by using its hydroxyls as ligands, and subsequently, a long chain structure is formed. The long chain structure not only can increase nucleation rate but also can control crystallite growth of $LiFePO_4$. As a result, it has a remarkable effect on decreasing the particle size of hydrothermally prepared $LiFePO_4$. On the other hand, this strong chelating ability is likely to lower its intrinsic degree of iron disorder in $LiFePO_4$,[14] potentially improving the electrochemical properties. Further investigation is in progress and will enable us to elucidate the mechanism for the enhancement of electrochemical performance.

Figure 8. Photographs of various samples: (a) original precursor, blue-green sticky liquid; (b) precursor hydrothermally reacted at 120 °C for 6 h, intermediate state; and (c) precursor reacted hydrothermally at 120 °C for 12 h, precipitated $LiFePO_4$ powder with yellowish supernatant.

3.7. Determination of Minimum Reaction Temperature. We tried to synthesize $LiFePO_4$ at various reaction temperatures below 120 °C. However, sticky precursor could not be dissolved at these temperatures. Finally, pure $LiFePO_4$ powders were successfully synthesized at 120 °C for 12 h. We found that $LiFePO_4$ powders prepared at 120 °C need longer time than those prepared at a higher temperature, suggesting that higher temperature can accelerate the dissolution and hydrolyzation of the precursor (Figure 8). In addition, it is found that $LiFePO_4$ has a similar formation rate to $LiMnPO_4$ under hydrothermal condition. These two olivine-type phases were all obtained in a very short reaction time in this study.

4. Discussion

Crystal Nucleation and Growth for $LiFePO_4$. On the basis of the XRD and FTIR results, accompanied with pH value evolution, morphology observations of each sample, and confirmation of dissolution−precipitation, a reasonable mechanism, involving three processes, is proposed for nucleation and crystal growth of $LiFePO_4$ under hydrothermal conditions, as schematically illustrated in Figure 9.

The first process is precursor dissolution. It is well-known that, at a higher temperature, the solubility of many compounds increases in water. Thus, with increasing temperature in reaction systems, all compounds in the precursor begin to dissolve and hydrolyze during the hydrothermal process, resulting in a decreasing pH value of solution. The concentrations of $[Fe(H_2O)_n]^{2+}$, $[Li(H_2O)_n]^{+}$, and PO_4^{3-}, then, build up in the reaction system.[42] This dissolution and hydrolytic process disaggregate agglomerated precursor into smaller aggregation (step1 ∼ step2).

The second process is nucleation. The change in the Gibbs free energy for the formation of crystalline nucleation on any surface that interacts with the nuclei is lower than that of the homogeneous nucleation mechanism. The surface free energies of the nucleation, under this mode, will be minimized so as to lower barrier for nucleation. This heterogeneous nucleation mechanism needs lower critical nucleation concentration than homogeneous nucleation.

Hence, when the heterogeneous critical nucleation concentration is reached,[43] those aquo−metal ions ($[Fe(H_2O)_n]^{2+}$, $[Li(H_2O)_n]^{+}$) and PO_4^{3-} in aqueous medium are transformed

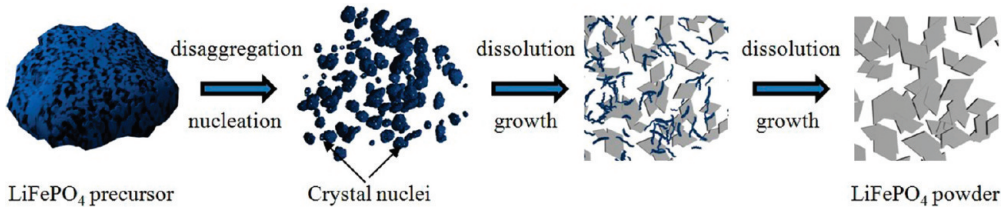

Figure 9. Schematic illustration for the nucleation and crystal growth of $LiFePO_4$ under hydrothermal conditions.

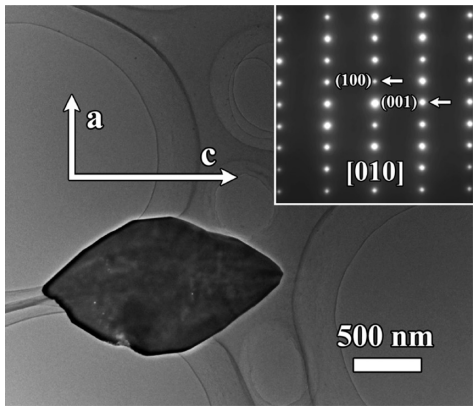

Figure 10. Typical TEM image of $LiFePO_4$ platelet and corresponding electron diffraction pattern (inset).

into a few $LiFePO_4$ nuclei at the surface or edge of the precursor, which are not completely dissolved in solution yet (step2). The undissolved precursor plasy a role as nucleating agent. The chemical reactions can be formulated as the following expression:

$$Fe^{2+} + Li^{+} + PO_4^{3-} \rightarrow LiFePO_4 \qquad (2)$$

The third process is nuclei growth. As the nucleation phase is not yet terminated, partial nuclei have stepped into crystal growth phase, leading to inhomogeneity of particle size of the $LiFePO_4$. Consequently, the hydrothermally prepared particles formed through a dissolution−precipitation mechanism have a wide particle size distribution [see Figure S5 (Supporting Information)]. In addition, crystal morphology is mainly controlled by anisotropy of nuclei surface energy in the micrometer range. Nuclei surfaces with high surface energy have greater ion adsorbing ability. Hence, as the reaction proceeded, the $LiFePO_4$ crystallite begins to grow up faster along the vertical directions of nuclei surfaces having high surface energy. At the same time, the undissolved precursors are dissolved to nanoleaflets (step2 ∼ step3). When the concentrations of $[Fe(H_2O)_n]^{2+}$, $[Li(H_2O)_n]^{+}$, and PO_4^{3-} in aqueous solution are lower than critical supersaturation concentration, the growth of $LiFePO_4$ is thus stopped (step 3 ∼ step 4).

The surface energy of the (010) plane for $LiFePO_4$ is smaller than that of other planes.[22] Therefore, as speculated from the proposed growth mechanism, the slowest [010] growth direction should be perpendicular to the largest facet of the platelike $LiFePO_4$. This has been experimentally proven in this study (see Figure 10), which is consistent with the previous report by Dokko et al.

From our experimentations and the discussion mentioned above, we comprehensively infer that supersaturation degree, pH value of reaction system, reaction medium, and total specific area of nucleating agents could influence the particle size and morphology of hydrothermally prepared $LiFePO_4$, which could finally produce an effect on its electrochemical performance.

5. Conclusions

A systematic investigation on the hydrothermal synthesis mechanism of $LiFePO_4$ has been carried out in this study. The results show that amorphous tetraphosphates are presented in $LiFePO_4$ precursor by analyzing the FTIR of samples and investigating the phase evolution of $LiMnPO_4$ synthesized hydrothermally. This compound undergoes hydrolysis via a hydrothermal route and provides PO_4^{3-} for the formation of crystalline $LiFePO_4$. Moreover, this hydrolytic process causes a remarkable decline of pH value in reaction medium. Three experimental observations provide strong evidence of dissolution−precipitation as the hydrothermal preparation mechanism of $LiFePO_4$. We believe that this work will enlighten a way to hydrothermally prepare phospholivines as positive electrode materials for the next generation of lithium-ion batteries that will be used in all-electric and plug-in HEV.

Acknowledgment. This work is supported by the Chinese Academy of Sciences and Institute of Metal Research, Chinese Academy of Sciences. We are also very grateful to Professor Masahiro Yoshimura from the Tokyo Institute of Technology for his instruction and help.

Supporting Information Available: Detailed FTIR spectra and XRD patterns of the $LiMnPO_4$ precursor and those reacted at various temperatures in oil bath; evolution of oil bath and in situ reaction temperatures with variation of pH values of supernatant liquid in synthesizing $LiMnPO_4$; typical SEM images of the $LiMnPO_4$ precursor, intermediate phase and aim-product $LiMnPO_4$; particle size distribution of $LiFePO_4$ prepared at different reaction medium; structure change of geometry of the anions tetraphosphates under hydrothermal condition from a metastable $P_4O_{12}^{4-}$ to $H_2PO_4^{-}$. This information is available free of charge via the Internet at http://pubs.acs.org.

References and Notes

(1) Padhi, A. K.; Nanjundaswamy, K. S.; Goodenough, J. B. *J. Electrochem. Soc.* **1997**, *144*, 1188.
(2) Yamada, A.; Chung, S. C.; Hinokuma, K. *J. Electrochem. Soc.* **2001**, *148*, A224.
(3) Huang, H.; Yin, S. C.; Nazar, L. F. *Electrochem. Solid-State Lett.* **2001**, *4*, A170.
(4) Wang, Y. Q.; Wang, J. L.; Yang, J.; Nu, Y. L. *Adv. Funct. Mater.* **2006**, *16*, 2135.
(5) Reimers, J. N.; Dahn, J. R. *J. Electrochem. Soc.* **1992**, *139*, 2091.
(6) Ohzuku, T.; Ueda, A. *J. Electrochem. Soc.* **1994**, *141*, 2972.
(7) Amatucci, G. G.; Tarascon, J. M.; Klein, L. C. *J. Electrochem. Soc.* **1996**, *143*, 1114.
(8) Chen, G. Y.; Song, X. Y.; Richardson, T. J. *Electrochem. Solid-State Lett.* **2006**, *6*, A295.
(9) Allen, J. L.; Jow, T. R.; Wolfenstine, J. *Chem. Mater.* **2007**, *19*, 2108.
(10) Dokko, K.; Koizumi, S.; Nakano, H.; Kanamura, K. *J. Mater. Chem.* **2007**, *17*, 4803.
(11) Yu, F.; Zhang, J. J.; Yang, Y. F.; Song, G. Z. *J. Mater. Chem.* **2009**, *19*, 9121.
(12) Huang, W. Q.; Qing, C.; Qin, X. *Russ. J. Electrochem.* **2010**, *46*, 359.

(13) Liu, H. P.; Wang, Z. X.; Li, X. H.; Guo, H. J.; Peng, W. J.; Zhang, Y. H.; Hu, Q. Y. *J. Power Sources* **2008**, *184*, 469.
(14) Chen, J. J.; Wang, S. J.; Whittingham, M. S. *J. Power Sources* **2007**, *174*, 442.
(15) Yang, S.; Zavalij, P. Y.; Whittingham, M. S. *Electrochem. Commun.* **2001**, *3*, 505.
(16) Chen, J. J.; Whittingham, M. S. *Electrochem. Commun.* **2006**, *8*, 855.
(17) Dokko, K.; Koizumi, S.; Sharaishi, K.; Kanamur, K. *J. Power Sources* **2007**, *165*, 656.
(18) Qian, J. F.; Zhou, M.; Cao, Y. L.; Ai, X. P.; Yang, H. X. *J. Phys. Chem. C* **2010**, *114*, 3477.
(19) Dokko, K.; Koizumi, S.; Kanamura, K. *Chem. Lett.* **2006**, *35*, 338.
(20) Chen, J. J.; Vacchio, M. J.; Wang, S. J.; Chernova, N.; Zavalij, P. Y.; Whittingham, M. S. *Solid State Ionics* **2008**, *178*, 1676.
(21) Shiraishi, K.; Dokko, K.; Kanamura, K. *J. Power Sources* **2005**, *146*, 555.
(22) Fisher, C. A. J.; Islam, M. S. *J. Mater. Chem.* **2008**, *18*, 1209.
(23) Recham, N.; Armand, M.; Laffont, L.; Tarascon, J. M. *Electrochem. Solid-State Lett.* **2009**, *12*, A39.
(24) Ellis, B.; Kan, W. H.; Makahnouk, W. R. M.; Nazar, L. F. *J. Mater. Chem.* **2007**, *17*, 3248.
(25) Hurowitz, J. A.; Tosca, N. J.; Dyar, M. D. *Am. Mineral.* **2009**, *94*, 409.
(26) Horchan, K.; Ferid, M.; Gacon, J. C.; Lecocq, S.; Malika, T. A.; Gregora, I. *Mater. Res. Bull.* **2002**, *37*, 1259.
(27) Ettis, H.; Naili, H.; Mhiri, T. *Cryst. Growth Des.* **2003**, *3*, 599.
(28) Chtioui, A.; BenHamada, L.; Jouini, A. *Mater. Res. Bull.* **2009**, *40*, 560.
(29) Sundarayya, Y.; Swamy, K. C. K.; Sunandana, C. S. *Mater. Res. Bull.* **2007**, *42*, 1942.
(30) Gangulibabu; Bhuvaneswari, D.; Kalaiselvi, N.; Jayaprakash, N.; Periasamy, P. *J. Sol-Gel Sci. Technol.* **2009**, *49*, 137.
(31) Koleva, V.; Zhecheva, E.; Stoyanova, R. *J. Alloys Compd.* **2009**, *476*, 950.
(32) Xiang, S. F.; Shen, Y. X.; Cao, T. B.; Guo, B. N. *Inorganic Chemistry*: Science Press: Beijing, 1998; Vol. 4, Chapter 13, pp 334.
(33) Xu, H. R.; Gao, L. *Mater. Lett.* **2002**, *57*, 490.
(34) Gao, S. S.; Zhou, Y. Y.; Li, H. X.; Li, X. Q. *China Powder Sci. Technol.* **2000**, *6*, s291.
(35) Zhang, L.; Chen, D. R.; Jiao, X. L. *J. Phys. Chem. B* **2006**, *110*, 2668.
(36) Xu, Z. P.; Lu, G. Q. *Chem. Mater.* **2005**, *17*, 1055.
(37) Pinceloup, P.; Courtois, C.; Vicens, J.; Leriche, A.; Thierry, B. *J. Eur. Ceram. Soc.* **1999**, *19*, 973.
(38) Zhou, Y. Y.; Gao, S. S.; Li, H. X.; Li, L. X. *China Powder Sci. Technol.* **2006**, *6*, s287.
(39) Hertl, W. *J. Am. Ceram. Soc.* **1988**, *71*, 879.
(40) Eckert, J. O.; Hung-Houston, C. C.; Gerston, B. L.; Lencka, M. M.; Riman, R. E. *J. Am. Ceram. Soc.* **1996**, *79*, 2929.
(41) Wang, Y. L.; Jiang, X. C.; Xia, Y. N. *J. Am. Chem. Soc.* **2003**, *125*, 16176.
(42) Livage, J.; Henry, M.; Sanchez, C. *Prog. Solid State Chem.* **1988**, *18*, 259.
(43) Lamer, V. K.; Dinegar, R. H. *J. Am. Chem. Soc.* **1950**, *72*, 4847.

JP104466E